Assessing the matrix effects on MALDI-MS in the positive and negative ion mode detection for protein-protected metal nanoclusters

Hao Yuan, Djibril Lima, Clothilde Comby-Zerbino, Charlène Bouanchaud, Fabien Chirot, Dipankar Bain, Sanjun Zhang, Rodolphe Antoine

Assessing the matrix effects on MALDI-MS in the positive and negative ion mode detection for protein-protected metal nanoclusters

Hao Yuan,[a] Djibril Lima,[a] Clothilde Comby-Zerbino,[a] Charlène Bouanchaud,[a] Fabien Chirot,[a] Dipankar Bain,[a] Sanjun Zhang [b,c] and Rodolphe Antoine [a,*]

a. Institut Lumière Matière UMR 5306, Université Claude Bernard Lyon 1, CNRS, Univ Lyon, F69100, Villeurbanne, France.

b. State Key Laboratory of Precision Spectroscopy, East China Normal University, No.500, Dongchuan Road, Shanghai, 200241, China

c. Collaborative Innovation Center of Extreme Optics, Shanxi University, Taiyuan, 030006, Shanxi, China.

Corresponding Author

* Rodolphe Antoine: rodolphe.antoine@univ-lyon1.fr

Abstract:

Protein-protected metal nanoclusters (MNCs) represent a new class of highly photoluminescent nanomaterials that have wide applications. Suitable reaction conditions combining protein and metal precursors can produce a vast range of different NC sizes. The average number of metal atoms per protein can be determined by mass spectrometry (MS). MS coupled with matrix-assisted laser desorption ionization (MALDI) presents a number of advantages such as detection with high sensitivity of nanoclusters with high molecular weights. Although many protein-protected MNCs have been characterized by MALDI-MS, a large dispersion in the number of metal atoms have been reported mainly due to sample preparation. In this work, we optimized the protocols for negative and positive ion detection mode as a general MALDI-MS sample preparation method for protein-protected MNCs (bovine serum albumin and lysozyme and with gold and silver). Negative and positive ion mode detection was compared, showing that negative ion mode detection in MALDI-MS can also be used with acidic matrices. Obvious matrix effects on ion signals and peak positions by MALDI-MS was observed. The average metal numbers of MNCs embedded in proteins are different depending on the MALDI matrix. The matrix effects give a warning for more serious consideration on MALDI-MS measurement and spectra analysis of MNCs.

Keywords:

protein-protected metal nanoclusters, matrix-assisted laser desorption ionization mass spectrometry, matrix effects, positive/negative ion mode detection

1 Introduction

Mass spectrometry (MS) has been a cornerstone in structure characterization of ligand-protected metal nanoclusters (MNCs) reaching atomic precision. [1-6] Indeed, MS can provide direct and accurate information on the composition of such MNCs, both in terms of the number of ligands and on the number of metal atoms. This is central to ensure for the atomic precision necessary to finely tuning the physico-chemical properties of the MNCs.[6-8] Yet in 1996, following the seminal Brust-Schiffrin synthesis method,[9] Whetten et al. pioneered the field of MS characterization of ultra-small nanoparticles, by using laser desorption ionization (LDI) to study dodecanethiol-protected gold nanoclusters (NCs) with masses in the range of 27–93 kDa.[10] Ionization techniques softer than LDI, especially matrix-assisted laser desorption ionization (MALDI) and electrospray ionization (ESI), later became more popular to better preserve intact ligand-protected clusters.[11, 12] As they rely on radically different ionization processes, these two techniques allow to address the diversity of the chemical nature of the ligands used to stabilize MNCs. ESI is particularly well-suited to ionize water soluble nanoclusters, and has the advantage to cause reduced fragmentation as compared to MALDI, even for fragile particles.[13] However, ESI usually yields multicharged species, resulting in more complex spectra. MALDI ionization is then popular to study nanoclusters with high molecular weights. For instance, it has been used to assign approximate compositions to very large nanoclusters with mass ranging from 300 to 400 kDa.[14, 15] In general MALDI performs better than ESI for organic-soluble nanoclusters, but the choice of the matrix is critical. For instance, Dass et al. proposed trans-2-[3-(4-tert-butylphenyl)-2-methyl-2-propenylidene] malononitrile (DCTB) as a matrix for MALDI-MS of intact $Au_{25}(PET)_{18}$ clusters.[16] Then Kawasaki and coworkers reported a new

MALDI matrix, e.g. α, β-diphenylfumaronitrile (DPF) for thiol-protected gold clusters.[17]

As biocompatibility is key to several applications of MNCs, recent strategies have been proposed to replace small organic thiolated ligands by macromolecular templates, like proteins.[18, 19] Bovine (or human) serum albumin BSA (HSA) and lysozyme proteins have been largely used as templates for directing MNCs, and some mass spectra were already published.[20] Actually, they are large enough to accommodate several metal atoms, allowing for producing highly luminescent species. Proteins not only stabilize the MNCs but also reduce the ions from metallic salts to MNCs, due to the presence of thiol groups.[21] The carboxyl and amino groups in proteins help to coordinate metal ions and subsequently accommodate atoms in the protein backbone.[22] Thus there is a simple correlation between the molecular weight of protein (MW), therefore the number of amino-acids, and the number of metal atoms. In the last few decades, other proteins (than BSA/HSA and lysozyme) such as chicken egg white, eggshell membrane, hemoglobin, ovalbumin, lactoferrin, keratin, lactalbumin, globulin, gluten and silk proteins have been used in the synthesis of MNCs.[19] But with such proteins, MNCs were produced without atomic precision (meaning that a distribution of metal atoms is observed), therefore their mass characterization was tricky or even not possible. Lysozyme and BSA were used in this work, because such proteins correspond to the lowest MW and highest MW respectively to produce MNCs with simple and reproducible protocols.

Since protein-protected MNCs are produced without atomic precision, for the nanocluster community, the most important information is the average number of metal atoms embedded in the protein templates, so commercial MALDI-TOF MS instrument in the linear mode is used, which is sufficient to address this point by comparing the mass addition of protein by encapsulating metal

atoms. Usually, protein-protected MNCs have been characterized by MALDI-MS using standard matrices compatible for proteins, such as sinapinic acid (SA), 2,5-dihydroxybenzoic acid (DHB), or α-cyano-α-hydroxy cinnamic acid (CHCA).[23-25] These matrices contain carboxylic groups favouring proton-transfer to the analyte, and thus the formation of protonated species. Even protein signal in negative mode using the same matrices have also been reported.[26] Consequently, most MS investigations of protein-protected clusters were performed in the positive ion mode. Besides, MALDI-MS investigations on BSA-protected gold nanoclusters using similar synthesis protocols led to some dispersion in the determination of the gold atoms number.[27] This dispersion may be influenced by sample preparation issues, e.g. use of different matrices and deposition protocols. The aim of the present work is to evaluate the effect of MALDI matrices for the MS characterization of protein-protected MNCs in both negative and positive ion modes. To this end, the MALDI response of a series of NCs of different metals, stabilized by different proteins, have been compared using different matrices.

2 Material and Methods

2.1 Chemical and reagents

Tetrachloroauric(III) acid ($HAuCl_4 \cdot 3H_2O$), bovine serum albumin (BSA), sinapinic acid (SA), 2,5-dihydroxybenzoic acid (DHB), alpha-Cyano-4-hydroxycinnamic (CHCA), trifluoroacetic acid (TFA) were purchased from Sigma-Aldrich. Silver nitrate ($AgNO_3$), Sodium borohydride ($NaBH_4$) were purchased from Acros Organics. Lysozyme from chicken egg white (14.3 kDa), acetonitrile (ACN) were purchased from Carl Roth. All chemicals were used

without further purification, and their solutions were prepared in MilliQ water (resistivity 18.2 MΩ).

2.2 Preparation of protein-protected nanoclusters

Three protein protected MNCs (BSA-AuNCs, BSA-AgNCs and Lysozyme-AuNCs) were prepared and the synthesis conditions were shown in Figure S1.

2.2.1. Synthesis of BSA-Protected Gold Nanoclusters

BSA-protected clusters were synthesizing as described by Xie et al.[23] Briefly, 5 mL of $HAuCl_4$ solution (10 mM) was mixed with 5 mL of BSA solution (50 mg/mL). The pH of the solution was then adjusted to 11 by adding 1 M NaOH solution and then left for 24 h at 37 °C. The clear brown solution of BSA-AuNCs was ultrafiltrated using a 50 kDa ultrafilter tube (GE Healthcare) against MilliQ water and was kept the same volume after purification. The final concentration of products is 23 mg/mL after purification by dry-weighting.

2.2.2. Synthesis of BSA-Protected Silver Nanoclusters

As previous synthesis,[28] aqueous solutions of $AgNO_3$ (1.6 mL, 7.5×10^{-3} M) and BSA (0.8 mL, 74 mg/mL) were mixed under vigorous stirring. After 2 min with white suspension, 0.08 mL of 1 M NaOH was added, and the solution turned to clear. Half an hour later, an aqueous solution of $NaBH_4$ (60 µL, 112 mM, dissolved in 0.1 M. NaOH) was added, and the reaction mixture immediately changed to dark brown. The stirring continued for 1 h at room temperature. Final solution was purified using a dialysis tubing (MWCO of 50kDa). The purified BSA-AgNCs with concentration of 21 mg/mL was stored in a 4 °C fridge for later use.

2.1.3. Lysozyme-Protected Gold Nanoclusters

Lysozyme-templated gold clusters was synthesized based on the previous report.[29] The final concentration was 150 μM and 0.625 mM for Lysozyme and Au^{3+}, respectively. The pH was adjusted to 12 using 1 M NaOH, after adding Au^{3+}. After 4 hours stirring at room temperature, red luminescence appeared, indicating the formation of clusters (see Figure 1). The solution was purified by a 3000 Da ultrafilter tube (Sartorius) with a raw concentration of 3.3 mg/mL.

2.3 Optical spectroscopy

Absorption and photoluminescence spectra were characterized for verifying the formation of same MNCs as reported (Figure 1). The molar concentration was estimated by the concentration of protein before synthesis reaction, based on an assumption that all added protein participated the formation of MNCs (concentration of BSA-AuNCs mother solution is 376 μM, concentration of BSA-AgNCs is 351 μM, and concentration of Lysoyme-AuNCs is 150 μM). For UV−vis absorption spectra, the samples were diluted with water to a final concentration of 10 μM and then were measured on an Avantes AvaSpec-2048 spectrophotometer with an AvaLight DH-S deuterium lamp with water as reference. Fluorescence emission and excitation spectra were recorded with a Horiba FluoroMax-4 spectrophotometer at excitation and emission slits of 5 nm bandpass. The samples were diluted with water to a final concentration of 20 μM. All measurements were conducted with a 1 cm quartz cuvette.

2.4 MALDI-TOF MS

MALDI-TOF MS analysis was conducted on ultrafleXtreme mass spectrometer (Bruker) in linear mode, equipped with 355 nm Nd:YAG laser. The signal was accumulated in 50000 shots; the intensity of the laser beam was the same in all experiments. MS instrument calibration was done with BSA (Sigma-Aldrich,

66431 Da), Insulin (Sigma-Aldrich, 5733.49 Da), Myoglobin (Sigma-Aldrich, 16952.30 Da) proteins in CHCA matrix. A groundsteel target was used.

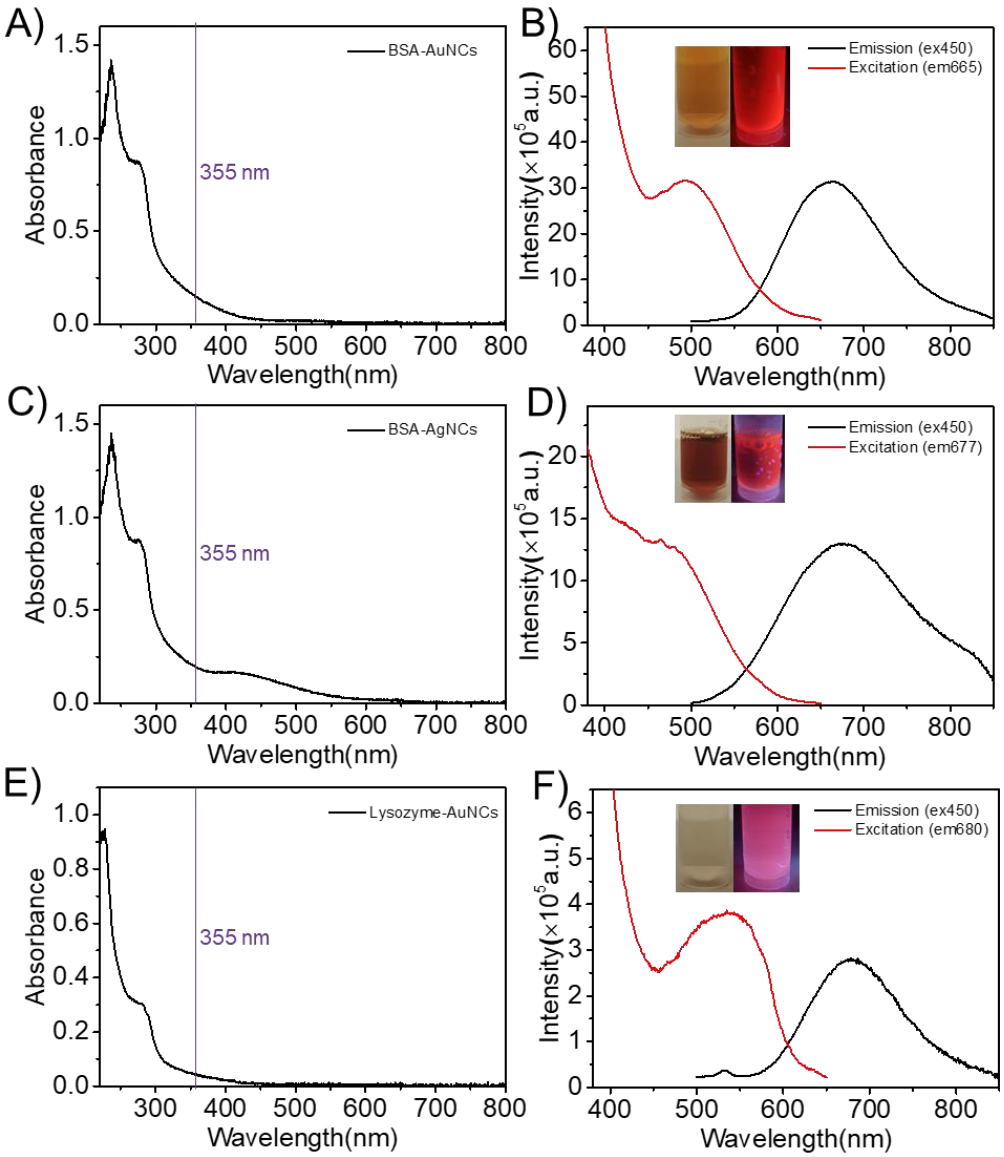

Figure 1. Absorption spectra of BSA-AuNCs (A), BSA-AgNCs (C), lysozyme-AuNCs (E) and photoluminescence emission and excitation spectra of BSA-AuNCs (B), BSA-AgNCs (D), lysozyme-AuNCs (F). Emission spectra were recorded with excitation wavelength at 450 nm and excitation spectra were measured with emission wavelength at 665 nm (BSA-AuNCs), 677 nm (BSA-AgNCs), 680 nm (Lysozyme-AuNCs). Insets: Nanoclusters photographs under day light and UV-light of 365 nm.

3 Results

Three protein-protected MNCs (BSA-AuNCs, BSA-AgNCs and Lysozyme-AuNCs) were prepared and their optical spectra are given in Figure 1. Protein-protected MNCs fluoresce in the red spectral region and the emission band at 600–800 nm with excitation maxima (at 450-550 nm).[20, 30]

3.1 Optimization of the sample preparation protocol for negative and positive ion mode

A critical step in MALDI MS is sample preparation. Unfortunately, the optimal way to obtain decent ion signal is highly dependent on the matrix and on the nature of the sample. We investigated different sample preparation strategies to optimize the response of the present protein-protected MNCs in the positive and negative mode using three matrices: SA, DHB, and CHCA. Table S1 summarizes the different conditions investigated based on BSA and BSA-AuNCs. Reproducibility of MALDI-MS results are summarized in Table S2.

To optimize MALDI protocols, we changed the concentration of analytes, the solvent, the matrix:analyte ratio and deposition structure (as exemplified in Fig. 2 for BSA-AuNCs). An intense peak at ~66 kDa corresponding to the singly charged 1+ ions is observed. Additional small peaks near 140000 m/z and at ~33 kDa correspond to dimer of BSA proteins and doubly charged 2+ ions of BSA respectively, as usually observed in MALDI-TOF MS measurements.[31, 32] First, MALDI-MS with different concentrations of MNCs were investigated (see Figure 2A), ranging from 6.7 μM to 33 μM. Then, different solvents used for both samples and matrix were investigated, with water-acetonitrile volume friction of 70/30 or 50/50, adding TFA or not (Figure 2B). Different methods were compared for the deposition, ranging from the co-deposition of a mixture of the MNCs and matrix solutions, to the depositions of different layers

alternating the matrix and the MNCs solutions (Figure 2C). Besides, we recorded the MALDI-MS spectra with different volume ratio of matrix to analyte (from 1:1 to 10:1) as shown in Figure 2D.

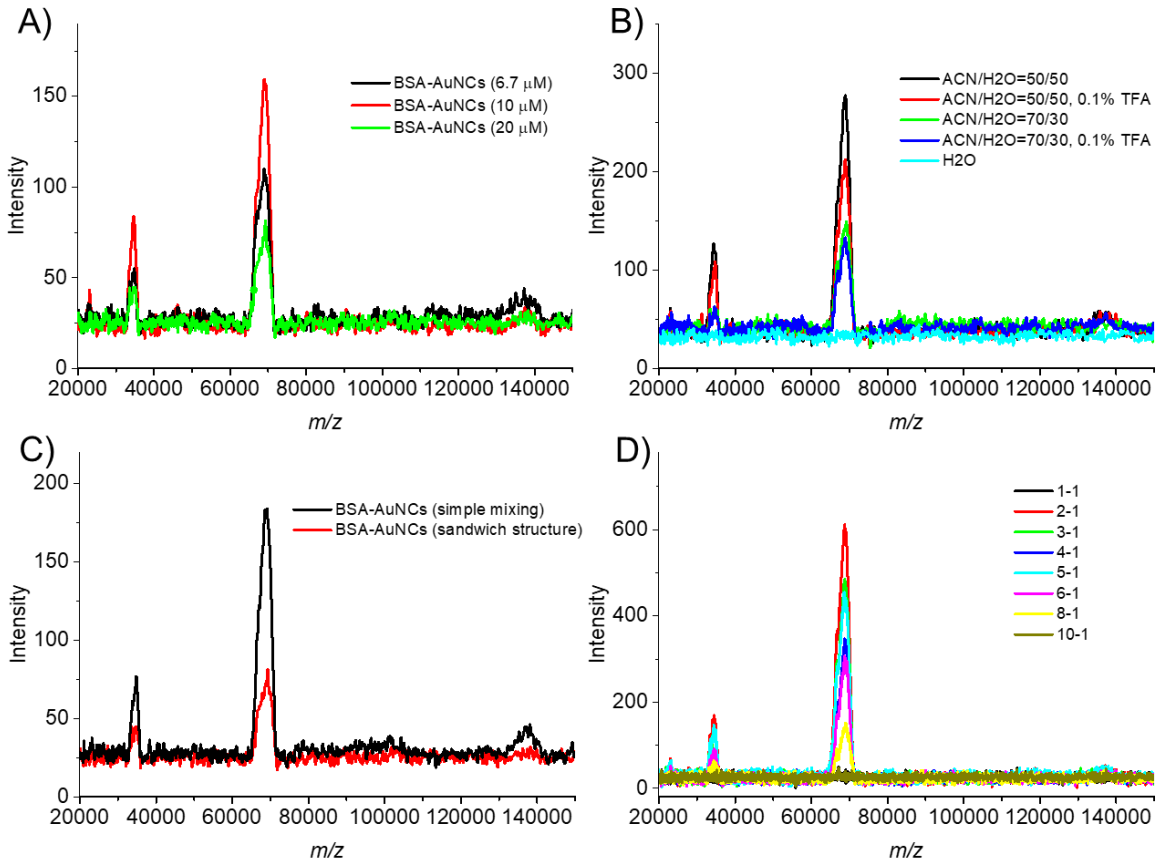

Figure 2. Mass spectra for BSA-AuNCs in negative ion mode using different deposition protocols (see table S1 for details on protocols). A: MALDI mass spectra with different concentration of BSA-AuNCs, corresponding to Test 2 in Table S1; B: MALDI mass spectra with different solvent, corresponding to Test 3 in Table S1; C: MALDI mass spectra with different deposition structure of simple mixing vs. layer-by-layer sandwich structure, corresponding to Test 2 and 3 in Table S1; D: MALDI mass spectra with different ratio of matrix to sample, corresponding to Test 4 in Table S1.

The optimal deposition protocol for both positive and negative mode was found to be as follow: The saturated CHCA, SA, DHB matrices solutions (16 mg/mL for CHCA, 33 mg/mL for SA, 100 mg/mL for DHB) were prepared in water-acetonitrile (50/50 vol.). 5 µL nanoclusters solution (30 µM in 50/50 water-

acetonitrile) was mixed with 10 µL saturated matrix under agitation (equivalent ratio 2:1). 1 µL of mixture was deposited to the groundsteel target with drying at ambient temperature.

3.2 Positive vs negative ion mode detection in MALDI-MS

MALDI matrices used in this work contain carboxylic groups favouring proton-transfer to the analyte, and thus the formation of protonated species. However, Cassady and coworkers nevertheless reported that peptides and proteins displayed good signals in the negative ion mode using acidic MALDI matrices.[26] The compelling advantages of negative ion mode detection in high-mass MALDI-MS were also emphasized for homomeric protein complexes.[33] This section aims at confirming previous measurements obtained on pure proteins with protein-protected MNCs and comparing the positive and negative mode MALDI-MS.

The optimized protocol described above was applied to all matrices and samples and MALDI-TOF spectra were collected both in the positive and negative ion mode. The intensities of 1 charge peak are compared in Fig. 3 for BSA-protected gold nanoclusters. Whatever the matrix, MALDI-TOF peaks for AuNCs in positive mode lead to a higher signal than in negative mode, in particular when CHCA is used as matrix. This strong difference in signal intensity regarding ionization modes in MALDI was already evidenced by previous studies on ion production for peptides and proteins.[26, 34]

3.3 Matrix effects on MALDI-MS in positive and negative mode

Interestingly and also unexpectedly, we can observe an obvious difference on the position of the peak in MALDI-MS corresponding to BSA-AuNCs mixed with three matrices (CHCA, SA, DHB), which means different gold number can be obtained with different matrices for the same sample. This is better

highlighted in Fig. 4 and Fig. S2 for BSA-protected gold nanoclusters in both negative and positive modes. As usually addressed for BSA-protected gold nanoclusters,[20] a broad mass distribution is observed corresponding to a distribution of the number of gold atoms in the protein template. While the width of the mass distribution is not too much affected by the nature of matrix, the average number of gold atoms (centre of the mass distribution) strongly depends on matrix. For instance, using CHCA the mass distribution is centred around m/z 68958, corresponding to an average of 12 Au atoms. In contrast, with DHB, the average mass is at m/z 70216, consistent with an average of 18 gold atoms attached to the protein. An intermediate result is obtained with SA.

As visible in Fig. 4 and Figure S2, the reduction in the average number of gold atoms in the protein is correlated to an increase of the intensity at the mass of bare BSA (m/z 66 500). The same trend is observed in both the positive and the negative ion mode. We tentatively interpret this correlation as the result of fragmentation of part of the protein-cluster complexes, leading to the loss of several neutral Au atoms, and eventually to the observation of bare BSA ions.

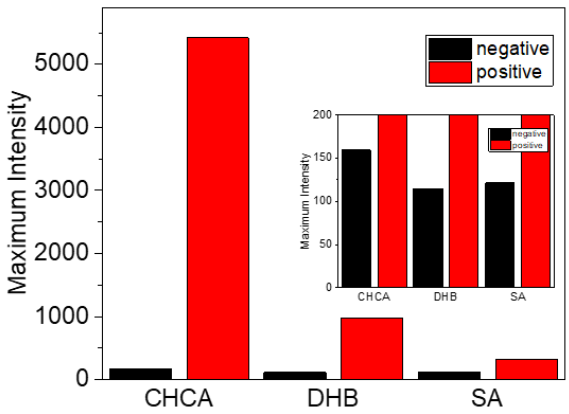

Figure 3. Maximum Intensity of 1 charge peak in MALDI-MS of BSA-AuNCs with different matrix (CHCA, SA, DHB) in negative ion mode detection vs. positive ion detection mode. Inset: Zoom-in image for comparison in negative mode.

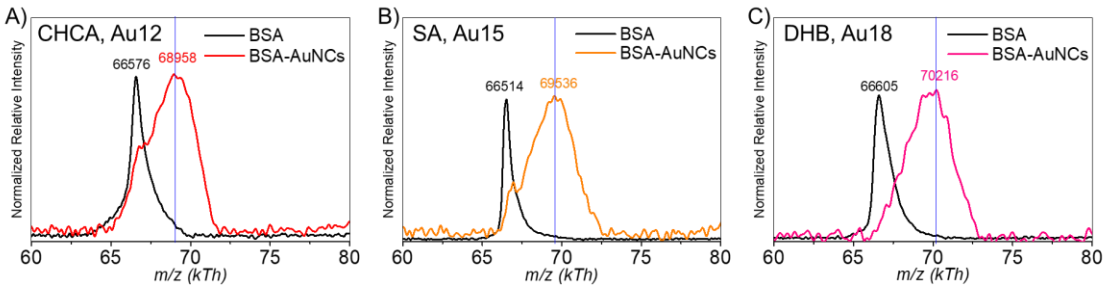

Figure 4. Normalized MALDI-TOF mass spectra in negative ion mode detection of BSA (black curve) and BSA-AuNCs with different matrix: CHCA (red curve), SA (orange curve), DHB (pink curve). The blue line corresponds to the m/z value of the intensity maximum of the distribution of BSA-AuNCs, with confirmation of 2-Gaussian fitting as described in Figure S4.

3.4 Matrix effects on MALDI-MS. Different metal and protein templates.

In order to evaluate how universal is the trend reported for positive and negative modes in MALDI-MS for BSA-AuNCs, we changed both the protein template (from BSA to lysozyme) and the nature of metal atoms (from gold to silver). Results are displayed in Fig. 5 (for BSA-AgNCs) and in Fig. 6 (for Lysozyme-AuNCs). As for gold clusters, the average number of silver atoms observed on BSA strongly depend on the matrix (Fig. 5). Moreover, reduced average number of Ag atoms on the protein also correlates with an increase of the signal of bare BSA. However, in the case of silver the highest number of Ag atoms is observed using SA (17 Ag atoms), while CHCA and DHB lead to the observation of significantly smaller species (9-10 Ag atoms).

When lysozyme is used as a scaffold for gold MNCs instead of BSA (Fig. 6), the number of Au atoms in the protein ranges from 1 to 5, thus significantly less than what was observed for BSA. The number of gold atom in protein is correlated to the size of the protein template from BSA (607 amino-acid residues) to lysozyme (only 130 amino-acid residues). While the max peak position seems similar, the width of the distribution for Lysozyme-AuNCs is

found to depend on the matrix. The width of the distribution is strongly decreased with CHCA as matrix, meaning that most probably evaporation of gold atoms has occurred.

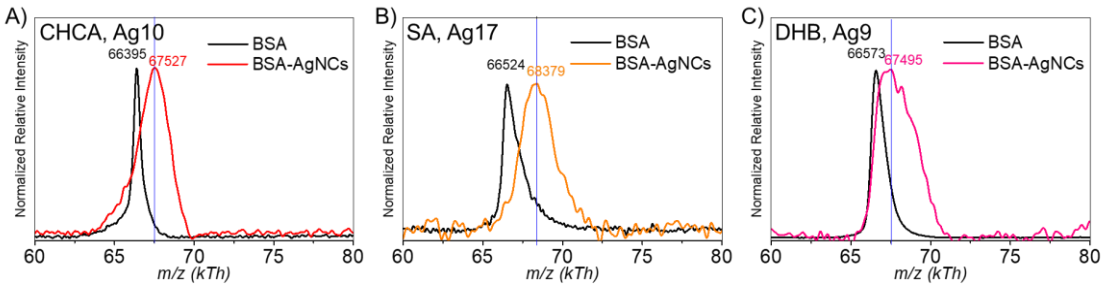

Figure 5. Normalized MALDI-TOF mass spectra in negative ion mode detection of BSA (black curve) and BSA-AgNCs with different matrix: CHCA (red curve), SA (orange curve), DHB (pink curve). The blue line corresponds to the m/z value of the intensity maximum of the distribution of BSA-AgNCs.

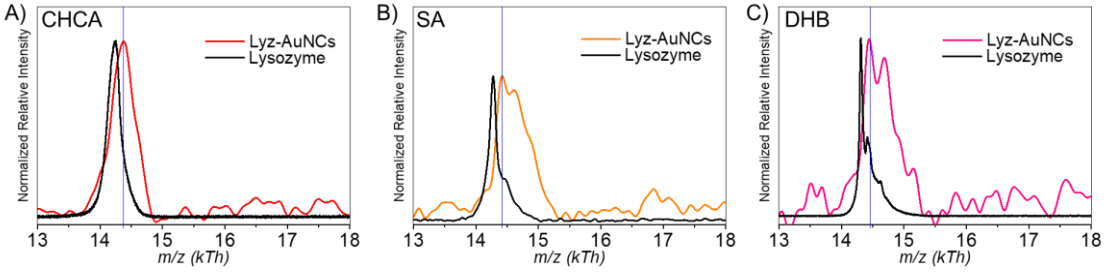

Figure 6. Normalized MALDI- TOF mass spectra in negative ion mode detection of Lysozyme (black curve) and Lysozyme-AuNCs with different matrix: CHCA (red curve), SA (orange curve), DHB (pink curve). The blue line corresponds to the m/z value of the intensity maximum of the distribution of Lysozyme-AuNCs

4 Discussion

CHCA, DHB, and SA are common matrices for MALDI largely used in peptide and protein analysis. The formation of protonated analytes is usually favoured since such matrices contain carboxylic groups, prone to act as proton donors. In the present study, we confirm that CHCA, DHB, and SA are useful for MALDI

in getting ion signal in protein-protected MNCs. Even if such matrices are acidic matrices, we provide supporting evidence for the formation of negative analyte ions in protein-protected MNCs (confirming what was already observed for bare proteins). However, the ion intensity obtained in negative mode are much lower than those reported for positive mode. Concerning processes for ionizing analytes with both ion polarity in MALDI, it was suggested that two matrix molecules were involved in the MALDI process and may yield a pair of protonated and deprotonated matrix ions that produce analyte molecules in protonation or deprotonation states.[35] Energy transfer process was also suggested, where following laser irradiation a nearby excited matrix molecule can transfer its energy to the analyte dimer through a short range energy transfer mechanism and trigger disproportionation, which leads to one protonated and one deprotonated analyte being produced simultaneously.[34] Proteins may have numerous acidic sites and may readily be deprotonated (see Table S3). Clearly similar processes are certainly occurring for protein-templated MNCs.

However, we would like to emphasize here that optical properties in bare proteins and in protein entrapping nanoclusters are drastically different. Indeed, proteins are mostly transparent to near-UV light (in particular at 355 nm), while protein-protected MNCs strongly absorb in the near-UV range (Figure 1). In particular, such MNCs present molar absorption coefficients similar to those of MALDI matrices (compare Tables S4 and S5). Thus, following laser irradiation, the internal energy in protein-templated MNCs is certainly higher than for bare proteins. This higher internal energy in the system may open new channels, in particular extensive metal atom evaporation. The Au-S bond dissociation is 3.2 eV,[36] while the Au-Au bond dissociation energy is only 2.3 eV.[37] Dissociation energies of gold clusters as a function of cluster size

are normally slightly higher than 3 eV.[38] The photon energy of the laser used in this study (355nm) is 3.49 eV.

We also reported in this study a strong matrix effect on the fragmentation in protein-templated MNCs. In particular, CHCA matrix lead to the observation of the stronger reduction of the average number of metal atoms in MNCs. This effect might be related to the very high molar absorption coefficients at 355 nm as compared to DHB and SA matrices. Also, we cannot exclude a matrix-dependent specific interaction with MNCs, probably related to crystallization/desolvation processes issues, facilitating energy transfer process.

While detailed information have been accumulated concerning structure–property relationships of atomically precise MNCs protected by small organic ligands (single crystal diffraction and theoretical prediction),[1] it is not the same case for protein-protected MNCs (due to the challenge of growing single crystals of protein-protected MNCs and limitations in computational chemistry). Structural motifs of nanoclusters in protein templates are not known and still under debate. Clearly, a better structure–property relationship of protein-protected MNCs is demanded and would help to better understand the observed strong matrix effect and the associated fragmentation processes.

In summary, the negative ion mode detection in MALDI-MS can also be a good way for addressing mass characterization of protein-protected MNCs in complement to positive ion detection mode. The optimal deposition protocol for both positive and negative mode was found to be as follow: The saturated CHCA, SA, DHB matrices solutions (16 mg/mL for CHCA, 33 mg/mL for SA, 100 mg/mL for DHB) were prepared in water-acetonitrile (50/50 vol.). 5 µL nanoclusters solution (30 µM in 50/50 water-acetonitrile) was mixed with 10 µL saturated matrix under agitation (equivalent ratio 2:1). 1 µL of mixture was deposited to the groundsteel target with drying at ambient temperature. DHB

matrix seems to be the optimal matrix for protein-protected gold nanoclusters, while SA matrix seems optimal for silver nanoclusters.

However, obvious matrix effects give a warning for more serious consideration on MALDI-MS measurement and spectra analysis of MNCs. This matrix effect is mainly due to the fact that MNCs strongly absorb in the near UV range. An alternative might be to use IR-MALDI-MS to efficiently desorb and ionize protein-protected MNCs without too much fragmentation with moderate laser fluence. Works under this line are currently implemented in our lab.

Declaration of Competing Interest

There are no conflicts to declare.

Acknowledgments

H.Y. is grateful for PhD fellowships donated by the China Scholarship Council (CSC). D.B. is grateful for post-doc fellowship donated by Agence Nationale de la Recherche (project MANBAMM, ANR-21-CE29-0020). C.B. is grateful for phD fellowship donated by Agence Nationale de la Recherche (project nanoGOLD, ANR-22-CE29-0022). R.A. S.Z. and H.Y. acknowledge Shanghai Science and Technology Innovation Program (22520712500) for support. R.A. and D.B. acknowledge Agence Nationale de la Recherche (project MANBAMM, ANR-21-CE29-0020) for support. R.A. D.L. and C.C.Z. acknowledge Agence Nationale de la Recherche (project MOONSTONE, ANR-22-CE42-0031) for support R.A. C.B. and F.C. acknowledge Agence Nationale de la Recherche (project nanoGOLD, ANR-22-CE29-0022) for support. This work was partially supported by the French region Rhônes Alpes Auvergne (Optolyse, CPER2016).

Appendix A. Supplementary data

All the data are presented in this article and the Supplementary Materials.

References

[1] R. Jin, C. Zeng, M. Zhou, Y. Chen, Atomically Precise Colloidal Metal Nanoclusters and Nanoparticles: Fundamentals and Opportunities, Chemical Reviews, 116 (2016) 10346–10413.

[2] I. Chakraborty, T. Pradeep, Atomically Precise Clusters of Noble Metals: Emerging Link between Atoms and Nanoparticles, Chemical Reviews, 117 (2017) 8208-8271.

[3] P. Chakraborty, T. Pradeep, The emerging interface of mass spectrometry with materials, NPG Asia Materials, 11 (2019) 48.

[4] C. Comby-Zerbino, X. Dagany, F. Chirot, P. Dugourd, R. Antoine, The emergence of mass spectrometry for characterizing nanomaterials. Atomically precise

nanoclusters and beyond, Materials Advances, 2 (2021) 4896-4913.
[5] Y. Lu, W. Chen, Application of Mass Spectrometry in the Synthesis and Characterization of Metal Nanoclusters, Analytical Chemistry, 87 (2015) 10659-10667.
[6] R. Antoine, Q. Yao, K. Yu, Looking for atomic precision in nanochemistry, Communications Chemistry, 7 (2024) 24.
[7] in: S. Thomas, K. Joseph, S. Appukuttan, M.S. Mathew (Eds.) Luminescent Metal Nanoclusters, Woodhead Publishing, 2022, pp. i-iii.
[8] in: T. Pradeep (Ed.) Atomically Precise Metal Nanoclusters, Elsevier, 2023, pp. i.
[9] M. Brust, M. Walker, D. Bethell, Schiffrin DJ and Whyman R, J. Chem. Soc. Chem. Commun., 1994 (1994) 801.
[10] R.L. Whetten, J.T. Khoury, M.M. Alvarez, S. Murthy, I. Vezmar, Z.L. Wang, P.W. Stephens, C.L. Cleveland, W.D. Luedtke, U. Landman, Nanocrystal gold molecules, Advanced Materials, 8 (1996) 428-433.
[11] T. Chen, Q. Yao, R.R. Nasaruddin, J. Xie, Electrospray Ionization Mass Spectrometry: A Powerful Platform for Noble-Metal Nanocluster Analysis, Angewandte Chemie International Edition, 58 (2019) 11967-11977.
[12] C. Kumara, V.R. Jupally, A. Dass, Gold Thiolate Nanomolecules: Synthesis, Mass Spectrometry, and Characterization, in: D.M.P. Mingos (Ed.) Gold Clusters, Colloids and Nanoparticles I, Springer International Publishing, Cham, 2014, pp. 155-187.
[13] R. Hamouda, F. Bertorelle, D. Rayane, R. Antoine, M. Broyer, P. Dugourd, Glutathione capped gold AuN(SG)M clusters studied by isotope-resolved mass spectrometry, International Journal of Mass Spectrometry, 335 (2013) 1-6.
[14] C. Kumara, M.M. Hoque, X. Zuo, D.A. Cullen, R.L. Whetten, A. Dass, Isolation of a 300 kDa, Au∼1400 Gold Compound, the Standard 3.6 nm Capstone to a Series of Plasmonic Nanocrystals Protected by Aliphatic-like Thiolates, The Journal of Physical Chemistry Letters, 9 (2018) 6825-6832.
[15] S. Vergara, U. Santiago, C. Kumara, D. Alducin, R.L. Whetten, M. Jose Yacaman, A. Dass, A. Ponce, Synthesis, Mass Spectrometry, and Atomic Structural Analysis of Au∼2000(SR)∼290 Nanoparticles, The Journal of Physical Chemistry C, 122 (2018) 26733-26738.
[16] A. Dass, A. Stevenson, G.R. Dubay, J.B. Tracy, R.W. Murray, Nanoparticle MALDI-TOF Mass Spectrometry without Fragmentation: Au25(SCH2CH2Ph)18 and Mixed Monolayer Au25(SCH2CH2Ph)18−x(L)x, Journal of the American Chemical Society, 130 (2008) 5940-5946.
[17] H. Kouchi, H. Kawasaki, R. Arakawa, A new matrix of MALDI-TOF MS for the analysis of thiolate-protected gold clusters, Analytical Methods, 4 (2012) 3600-3603.
[18] X. Meng, I. Zare, X. Yan, K. Fan, Protein-protected metal nanoclusters: An emerging ultra-small nanozyme, WIREs Nanomedicine and Nanobiotechnology, 12

(2020) e1602.
[19] I. Zare, D.M. Chevrier, A. Cifuentes-Rius, N. Moradi, Y. Xianyu, S. Ghosh, L. Trapiella-Alfonso, Y. Tian, A. Shourangiz-Haghighi, S. Mukherjee, K. Fan, M.R. Hamblin, Protein-protected metal nanoclusters as diagnostic and therapeutic platforms for biomedical applications, Materials Today, 66 (2023) 159-193.
[20] P.L. Xavier, K. Chaudhari, A. Baksi, T. Pradeep, Protein-protected luminescent noble metal quantum clusters: an emerging trend in atomic cluster nanoscience, Nano Reviews, 3 (2012) 14767.
[21] R. Antoine, D. Maysinger, L. Sancey, V. Bonačić-Koutecký, Open questions on proteins interacting with nanoclusters, Communications Chemistry, 5 (2022) 47.
[22] J.M. Dixon, S. Egusa, Conformational Change-Induced Fluorescence of Bovine Serum Albumin–Gold Complexes, Journal of the American Chemical Society, 140 (2018) 2265-2271.
[23] J. Xie, Y. Zheng, J.Y. Ying, Protein-Directed Synthesis of Highly Fluorescent Gold Nanoclusters, Journal of the American Chemical Society, 131 (2009) 888-889.
[24] P. Chakraborty, T. Pradeep, Chapter 10 - Mass spectrometry of atomically precise clusters, in: T. Pradeep (Ed.) Atomically Precise Metal Nanoclusters, Elsevier, 2023, pp. 203-227.
[25] F. Bertorelle, K.D. Wegner, M. Perić Bakulić, H. Fakhouri, C. Comby-Zerbino, A. Sagar, P. Bernadó, U. Resch-Genger, V. Bonačić-Koutecký, X. Le Guével, R. Antoine, Tailoring the NIR-II Photoluminescence of Single Thiolated Au25 Nanoclusters by Selective Binding to Proteins**, Chemistry – A European Journal, 28 (2022) e202200570.
[26] J. Gao, C.J. Cassady, Negative ion production from peptides and proteins by matrix-assisted laser desorption/ionization time-of-flight mass spectrometry, Rapid Communications in Mass Spectrometry, 22 (2008) 4066-4072.
[27] Y.-C. Hsu, M.-J. Hung, Y.-A. Chen, T.-F. Wang, Y.-R. Ou, S.-H. Chen, Identifying Reducing and Capping Sites of Protein-Encapsulated Gold Nanoclusters, Molecules, 24 (2019) 1630.
[28] Y. Yu, J. Geng, E.Y.X. Ong, V. Chellappan, Y.N. Tan, Bovine Serum Albulmin Protein-Templated Silver Nanocluster (BSA-Ag13): An Effective Singlet Oxygen Generator for Photodynamic Cancer Therapy, Advanced Healthcare Materials, 5 (2016) 2528-2535.
[29] A. Baksi, P.L. Xavier, K. Chaudhari, N. Goswami, S.K. Pal, T. Pradeep, Protein-encapsulated gold cluster aggregates: the case of lysozyme, Nanoscale, 5 (2013) 2009-2016.
[30] A. Soleilhac, F. Bertorelle, R. Antoine, Sizing protein-templated gold nanoclusters by time resolved fluorescence anisotropy decay measurements, Spectrochimica Acta Part A: Molecular and Biomolecular Spectroscopy, 193 (2018) 283-288.

[31] M. Nešić, I. Popović, A. Leskovac, M. Petković, Biological activity and binding properties of [Ru(II)(dcbpy)2Cl2] complex to bovine serum albumin, phospholipase A2 and glutathione, BioMetals, 29 (2016) 921-933.

[32] H. Choi, D. Lee, Y. Kim, H.-Q. Nguyen, S. Han, J. Kim, Effects of Matrices and Additives on Multiple Charge Formation of Proteins in MALDI–MS Analysis, Journal of The American Society for Mass Spectrometry, 30 (2019) 1174-1178.

[33] S. Mädler, K. Barylyuk, E. Boeri Erba, R.J. Nieckarz, R. Zenobi, Compelling Advantages of Negative Ion Mode Detection in High-Mass MALDI-MS for Homomeric Protein Complexes, Journal of The American Society for Mass Spectrometry, 23 (2012) 213-224.

[34] W.C. Chang, L.C.L. Huang, Y.-S. Wang, W.-P. Peng, H.C. Chang, N.Y. Hsu, W.B. Yang, C.H. Chen, Matrix-assisted laser desorption/ionization (MALDI) mechanism revisited, Analytica Chimica Acta, 582 (2007) 1-9.

[35] K. Breuker, R. Knochenmuss, R. Zenobi, Proton transfer reactions of matrix-assisted laser desorption/ionization matrix monomers and dimers, Journal of the American Society for Mass Spectrometry, 10 (1999) 1111-1123.

[36] D.L. Kokkin, R. Zhang, T.C. Steimle, I.A. Wyse, B.W. Pearlman, T.D. Varberg, Au–S Bonding Revealed from the Characterization of Diatomic Gold Sulfide, AuS, The Journal of Physical Chemistry A, 119 (2015) 11659-11667.

[37] R. Grande-Aztatzi, P.R. Martínez-Alanis, J.L. Cabellos, E. Osorio, A. Martínez, G. Merino, Structural evolution of small gold clusters doped by one and two boron atoms, Journal of Computational Chemistry, 35 (2014) 2288-2296.

[38] M. Vogel, K. Hansen, A. Herlert, L. Schweikhard, Model-Free Determination of Dissociation Energies of Polyatomic Systems, Physical Review Letters, 87 (2001) 013401.